Nguyen, D. H., Goman, M., Lowenberg , M. H., & Neild, S. A. (2022). Evaluating Longitudinal Unsteady Aerodynamic Effects in Stall for a T-Tail Transport Model. *Journal of Aircraft*, *59*(4), 964-976. https://doi.org/10.2514/1.C036622

Evaluating Longitudinal Unsteady Aerodynamic Effects in Stall for a T-Tail Transport Model

Duc H. Nguyen[1]
University of Bristol, Bristol, BS8 1TR, United Kingdom

Mikhail G. Goman[2]
De Montfort University, Leicester, LE1 9BH, United Kingdom

Mark H. Lowenberg[3] and Simon A. Neild[4]
University of Bristol, Bristol, BS8 1TR, United Kingdom

Although there have been many proposed methods to model unsteady aerodynamic effects in the stall and post-stall region, little work has been done to directly assess the impact of unsteady aerodynamic models on stability and control characteristics. In this paper, we combine the state-space method for unsteady aerodynamic modelling with bifurcation analysis to examine the sensitivity of stall and post-stall behaviour to the choice of aerodynamic modelling method: quasi-steady or unsteady. It is found that quasi-steady modelling can adequately capture the dynamics of the chosen example of a T-tailed transport aircraft with negligible wing-tail coupling. The study is then expanded to investigate a hypothetical situation with highly unsteady aerodynamic characteristics resembling a delta wing configuration – achieved by increasing the time delay constants in the unsteady model. This results in an aircraft with significantly lower flying qualities as indicated by bifurcation analysis. These findings highlight the need to implement unsteady aerodynamic modelling techniques in high-performance aircraft with significant vortex-related unsteady aerodynamics in order to sufficiently capture their stall and post-stall dynamics.

[1] Research Associate, Department of Aerospace Engineering. Student Member AIAA.
[2] Professor of Dynamics, School of Engineering and Sustainable Development. Senior Member AIAA.
[3] Professor of Flight Dynamics, Department of Aerospace Engineering. Senior Member AIAA.
[4] Professor of Nonlinear Structural Dynamics, Department of Aerospace Engineering.

I. Introduction

Quasi-steady aerodynamic modelling remains the most popular method for representing aerodynamic forces and moments in flight dynamics studies. This method is traditionally based on the use of stability and control derivatives, which can adequately model the nonlinearities at low angles-of-attack during normal flights [1]. In the stall and post-stall regime, however, quasi-steady modelling cannot adequately capture many important phenomena due to the major influence of unsteady (time-dependent) effects in these regions, which only become noticeable when the aircraft is manoeuvring. In fact, it has been shown that these unsteady effects can lead to strong discrepancies between the behaviours predicted using best-practice wind-tunnel tests and actual test flights [2]. Many important stall and post-stall flight characteristics cannot be adequately analysed as a result, which can affect further studies of highly manoeuvrable combat aircraft as well as of upsets and loss-of-control prevention in transport applications [3-5].

The need for adequate account for time-dependent flow phenomena is now recognised, and various methods to model these unsteady aerodynamics effects have been proposed as a result [6, 7]. However, most of the published studies on the topic only focus on accurate modelling of variations in the force and moment coefficients under wind-tunnel-like tests conditions, and no investigation has directly established the link between unsteady aerodynamics and flying characteristics in terms of stability and control. As observed in the real world, the presence of these time-dependent phenomena can seriously degrade the handling qualities of the aircraft in stall and post-stall regions [2]. A further study that constructs the basic framework to combine unsteady aerodynamics with stability and control analysis is therefore necessary.

One of the common methods for investigating nonlinearities in flight dynamics is bifurcation analysis. Since its first application in the early 80s [8, 9], the method has been recognised by both researchers and the industry for its capability of characterising many important phenomena encountered at high angles-of-attack and sideslip, such as spin, wing rock, and static hysteresis. This makes bifurcation analysis a popular choice for studying the behaviours of high-performance fighter jets [10, 11] as well as transport aircraft in upsets and loss-of-control situations [12, 13]. It has also been used for the study of rotorcraft, where the periodic nature of rotor behaviour in forward flight are facilitated via the use of harmonic forcing [14]. Recent works have extended this form of bifurcation analysis to assess the flight dynamics of fixed-wing aircraft under an external harmonic forcing term [15, 16]. Referred to as ‘nonlinear frequency

analysis' or 'harmonically-forced bifurcation analysis', this approach permits the construction of a Bode plot without relying on linearisation and transfer functions – therefore allowing the non-stationary nonlinear effects such as sub- and super-harmonic resonance [15] and actuator rate limiting [16] to be directly reflected in the frequency response. Such nonlinear frequency responses can be constructed from time simulations but this is time-consuming and unstable solutions are unlikely to be identified in this manner. In the context of unsteady aerodynamic analysis, nonlinear frequency response is an especially suitable tool because a harmonically-forced aircraft is non-stationary by nature, meaning that the time-dependent aerodynamic effects observed during the aircraft's transient motion can be directly reflected in the analysis. As a result, the insights gained by nonlinear frequency analysis cannot be obtained from linear-based methods or conventional (unforced) bifurcation analysis due to their linear and stationary nature, respectively.

To initiate work on the topic, this paper utilised bifurcation analysis to examine the effect of unsteady aerodynamics on the longitudinal dynamics of the NASA GTT (Generic T-tail Transport) airliner model. Specifically, we use both conventional bifurcation analysis and the nonlinear frequency response to assess the sensitivity of stall and post-stall behaviours to the choice of aerodynamic modelling method: quasi-steady or unsteady. The GTT is of interest in the context of stall and upset dynamics following incidents such as the fatal Colgan Air crash of a (T-tailed) Bombardier DHC-8-400 in 2009. The accident report [17] quotes the probable cause as "inappropriate response to the activation of the stick shaker, which led to an aerodynamic stall from which the airplane did not recover" and recommends the incorporation of realistic, fully developed stall models into training simulators.

The GTT model was generated from wind tunnel test data by NASA and Boeing [18-20] from both static and forced oscillation tests, resulting in a nonlinear but conventional (quasi-steady) flight dynamics model. Further studies were conducted using computational fluid dynamics to establish the effects of Reynolds number on aerodynamics up to and including the post-stall region [21]. In this paper, we augment the quasi-steady aerodynamics in the GTT model provided by NASA Langley (which covers an angle of attack range of -8^{o} to $+60^{o}$ and sideslip $\pm 35^{o}$) with unsteady aerodynamics effects using the state-space method, sometimes referred to as the Goman-Khrabrov model in the literature [22]. The objective is to compare the two aerodynamic modelling techniques and validate the capability of the state-space approach in matching the forced oscillation test results. Finally, the study is expanded to consider a

hypothetical highly-unsteady version of the GTT by artificially increasing the magnitude of delay-relaxation parameters to the values typical of a delta wing configuration [23]. This allows us to demonstrate the advantages of our proposed approach when studying transient dynamics while also providing speculative insights into the impact of strong unsteady effects on the flight dynamics and control.

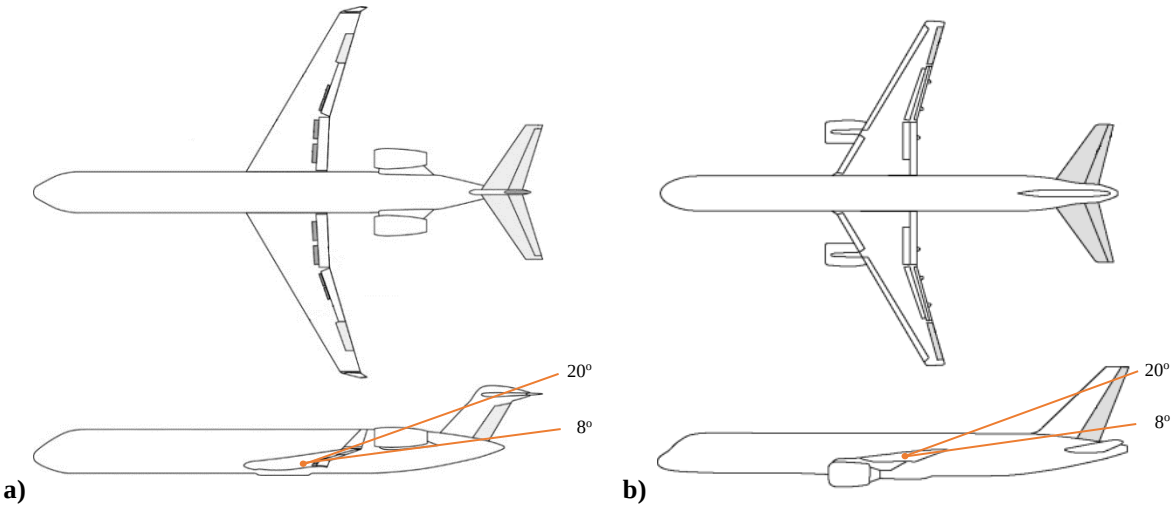

Fig. 1 The NASA GTT (a) and GTM (b) with approximate wake geometry for angles of attack 8° and 20°.

Image sources: [5, 19]

The implementation of a state-space model that represents aerodynamic time dependence is well established for lift. However, for pitching moment it becomes more difficult if there is interaction between the wing wake and the horizontal tailplane over the angle of attack range at which separated flow unsteadiness is significant (the stall region). Fig. 1 shows the geometries of the GTT and also the GTM (Generic Transport Model) – another NASA configuration that has been studied extensively in te rms of upset behaviour, and which has underwing-mounted engines and a low horizontal tail. It also indicates the geometric location of the wake of both configurations in the stall region. Fig. 1a indicates that the horizontal stabiliser of the GTT is above the wing wake, particularly when wing downwash is accounted for. For the low-tail GTM, however, the wake is likely to impinge on the horizontal tailplane, due to downwash, therefore affecting the separated-flow unsteady aerodynamics. The wing-tail coupling is significant in this instance and therefore must be included in the analysis [24, 25]. For the GTT, on the other hand, it is acceptable when modelling the state-space pitching moment to assume that there is negligible wing-tail coupling and that the nonlinear unsteady aerodynamics is able to be fully described in terms of the flow separation process over the wing. This

assumption for a T-tail aircraft may be further justified by the fact that the time scales identified for the NASA GTT will be shown to match very well with the time scales obtained for the NASA Common Research Model (CRM) wing-body-notail configuration [26]. This is discussed in more detail in section II-C.

II. Modelling and Validation

The first mathematical formulation of the aeroplane's longitudinal dynamics was introduced in 1911 by Bryan, where the aerodynamic derivatives in the equations of motion were treated as constant coefficients [1]. This was later expanded to accommodate flights at different conditions by considering these coefficients to be functions of the angles of attack (and often other states such as speed or Mach number, and of control surface deflections such as elevator δ_e); forces and moments under transient conditions, including time lag for wing downwash to reach the tailplane, were approximated by stability derivatives as a function of angular rate and rate of change of angle of attack. This is the so-called quasi-steady modelling method. Despite its role as the foundation for modern flight dynamics and control analyses [3], it is known that the quasi-steady method cannot accurately model the unsteady aerodynamic effects in the stall region, such as delayed flow attachment and separation. In these instances, the state-space aerodynamic modelling method has been shown to be a better way to reflect these phenomena [22]. The formulation and implication of both approaches are discussed in this section.

A. Quasi-Steady Modelling

As mentioned, the aerodynamic coefficients in the nonlinear quasi-steady approach are functions of the angle of attack and sometimes other motion and/or control variables. Their nonlinear relationships under static conditions are usually measured in wind tunnel static tests or predicted computationally, in either case keeping the angle of attack and sideslip angle constant. The contributions to aerodynamic loads due to the pitch rate q and rate of change in the angle of attack $\dot{\alpha}$ are usually considered as a linear increment by adding aerodynamic rotary or acceleration derivatives, also as a function of angle of attack. If only the longitudinal motion is considered, the normal force and pitching moment coefficients C_z and C_m can be represented in the following form:

$$C_z = C_{z,st}(\alpha) + C_{zq}(\alpha)\frac{qc}{2V} + C_{z\dot{\alpha}}(\alpha)\frac{\dot{\alpha}c}{2V} + C_{z\delta_e}(\alpha)\delta_e \quad (1)$$

$$C_m = C_{m,st}(\alpha) + C_{mq}(\alpha)\frac{qc}{2V} + C_{m\dot{\alpha}}(\alpha)\frac{\dot{\alpha}c}{2V} + C_{m\delta_e}(\alpha)\delta_e \quad (2)$$

where the first terms in equations (1) and (2) are the static nonlinear dependencies on the angle of attack obtained from static wind tunnel tests; the linear terms representing rotary (q) and acceleration aerodynamic derivatives ($\dot{\alpha}$) are normally obtained in wind tunnel forced oscillations tests, while control derivatives are calculated based on linearisation of the experimental nonlinear dependences from static tests. The experimental forced oscillation rigs normally involve pure angular oscillations so that pitch rate q and the rate of change in angle of attack $\dot{\alpha}$ are identical. This leads to the measurement of rotary and unsteady aerodynamic derivatives as mixed combinations, for example, $C_{zq}(\alpha) + C_{z\dot{\alpha}}(\alpha)$ and $C_{mq}(\alpha) + C_{m\dot{\alpha}}(\alpha)$. Experimental rigs capable of generating heave motions for separate measurement of these two aerodynamic derivatives exist but are not widely used. As a compromise, representations (1) and (2) are often modified by inclusion of the measured cumulative pairs $C^*_{zq} = C_{zq}(\alpha) + C_{z\dot{\alpha}}(\alpha)$, $C^*_{mq} = C_{mq}(\alpha) + C_{m\dot{\alpha}}(\alpha)$, which is partly justified by noting that the changes in airplane stability characteristics due to the use of cumulative pairs are slight. This results in the following simplified representation:

$$C_z = C_{z,st}(\alpha) + C^*_{zq}(\alpha)\frac{qc}{2V} + C_{z\delta_e}(\alpha)\delta_e \quad (3)$$

$$C_m = C_{m,st}(\alpha) + C^*_{mq}(\alpha)\frac{qc}{2V} + C_{m\delta_e}(\alpha)\delta_e \quad (4)$$

Issues arise when the rotary/unsteady aerodynamic derivatives are measured at stall conditions. This is caused by the flow separation creating a dependency of the measured aerodynamic derivatives on the frequency ω and amplitude of forced oscillations:

$$C_z = C_{z,st}(\alpha) + C^*_{zq}(\alpha,\omega)\frac{qc}{2V} + C_{z\delta_e}(\alpha)\delta_e \quad (5)$$

$$C_m = C_{m,st}(\alpha) + C^*_{mq}(\alpha,\omega)\frac{qc}{2V} + C_{m\delta_e}(\alpha)\delta_e \quad (6)$$

The flow separation may also cause a divergence in the effects of pitch and heave, in which case the use of combined derivatives C_{zq}^* and C_{mq}^* becomes less justifiable.

It is not possible to directly translate these frequency and amplitude dependencies into time simulation of free flights involving arbitrary motions. This can be partially resolved by replacing the dependence on the frequency ω with the dependence on the angular pitching velocity q, as was done in [18, 20].

B. State-Space Method for Unsteady Aerodynamic Modelling

The state-space method provides a more accurate representation of the unsteady aerodynamic effect in the normal force coefficient C_z [22-24]. Recent development has shown that this approach is successful in modelling the effects of blowing-type plasma actuators for active control of flow separation as well as vertical wind gusts [27, 28]. At its core, the state-space method uses two separate envelope functions $C_{z,att}(\alpha)$ and $C_{z,sep}(\alpha)$ to describe the dependencies of attached and fully separated flow on the angle of attack, plus an internal state variable x_z characterising the delayed transition between $C_{z,att}(\alpha)$ and $C_{z,sep}(\alpha)$. This delay and relaxation process is reflected by a first-order lag in x_z, which includes two time constants: T_1 characterising the flow relaxation process and T_2 characterising the delay in flow separation due to the rate of change in angle of attack ($\dot{\alpha}$). Accordingly, the unsteady model for normal force coefficient C_z can be represented in the following form:

$$C_z = C_{z,att}(\alpha)x_z + C_{z,sep}(\alpha)(1 - x_z) + C_{zq0}(\alpha)\frac{qc}{2V} + C_{z\delta_e}(\alpha)\delta_e \tag{7}$$

$$T_1\frac{dx_Z}{dt} + x_z = x_{z0}(\alpha - T_2\dot{\alpha} - \Delta\alpha_{Re}) \tag{8}$$

where:

- $C_{z,att}(\alpha)$ is the dependence of the normal force coefficient assuming that flow is attached
- $C_{z,sep}(\alpha)$ is the dependence of the normal force coefficient assuming that flow is fully separated
- $x_z \in [0,1]$ is a normalised internal state variable characterising transition from attached to separated flow

- $x_{z0}(\alpha)$ is a smooth function describing transition between the attached and separated flow so that $x_{z0} = 1$ at angles of attack below the stall zone and $x_{z0} = 0$ at angles of attack above the stall zone
- T_1 is physical time in seconds characterising the relaxation process; it is often expressed as non-dimensional relaxation time $\tau_1 = T_1 V/c$
- T_2 is physical time in seconds characterising the delay in onset of flow separation; it is often expressed in non-dimensional form as $\tau_2 = T_2 V/c$
- $\Delta\alpha_{Re}$ is the change in angle of attack arising from the effect of Reynolds [22]; a similar adjustment can be made to capture the intensity of jet blowing [27] or vertical wind gust w [28] when present
- C_{zq0} is the rotary aerodynamic derivative reflecting contribution from an airframe without account for flow separation on the wing
- $C_{z\delta_e}$ is the aerodynamic control derivative with respect to elevator deflection.

It should be noted that x_z is an important feature of the state-space formulation: it can be related, directly or indirectly, to the flow physics and, consequently, its value and dynamical behaviour carry a physical meaning. A Reynolds number adjustment, $\Delta\alpha_{Re}$, is not implemented in the current work as the sub-scale wind tunnel model data is used.

Unsteady aerodynamic modelling in pitching moment is more complicated because the process depends on both the magnitude of the aerodynamic force C_Z and the centre of its application x_p [24]. Nevertheless, a structure similar to equations (7) and (8) can still be used on a T-tail aircraft because, as explained in Section I, the wing-tail interaction in the stall region is minimal (α between 8° and 20°)and hence will not influence the aerodynamic pitching moment. This is contrary to the conventional (low tail) configuration, where both the development of flow separation on the wing and the delayed action of wing downwash on the horizontal tail must be considered [5].

Accordingly, the contribution to the moment coefficient from flow separation on the wing can be described by a smooth function $C_{m,ws}(\alpha)$, which equals zero outside of the stall region, and results in the following unsteady representation of the pitching moment coefficient:

$$C_m = C_{m0}(\alpha) + x_m + C_{mq0}(\alpha)\frac{qc}{2V} + C_{m\delta_e}(\alpha)\delta_e \tag{9}$$

$$T_1\frac{dx_m}{dt} + x_m = C_{m,ws}(\alpha - T_2\dot{\alpha} - \Delta\alpha_{Re}) \tag{10}$$

where:

- $C_{m0}(\alpha), C_{m,ws}(\alpha)$ are the functions describing static dependence of the pitching moment coefficient without account of flow separation over the wing and the contribution from the wing separation to the pitch break, respectively. The sum of these two functions should be equal to the static dependence $C_{m,st}(\alpha) = C_{m0}(\alpha) + C_{m,ws}(\alpha)$
- $x_m(t)$ is the state variable characterising dynamic contribution to the pitching moment coefficient
- C_{mq0} is the rotary aerodynamic derivative reflecting contribution from an airframe without account of flow separation on the wing

Fig. 2a and 2b illustrate the contributions of the static terms in equations (7-8) and (9-10) to the normal force and pitching moment coefficients of the GTT airplane, respectively. Using our proposed modelling method, $C_{m,ws}(\alpha)$ captures the nonlinear change in pitching moment in the stall region, which is characterised by the onset of an unstable positive slope and subsequent restoration of a negative slope. A similar process can be used for the initial choice of functions $C_{zq0}(\alpha)$ and $C_{mq0}(\alpha)$. This methodology could be extended to low-tail geometries by considering aerodynamic coefficients for different wing-body-tail, wing-body, and body-tail combinations, obtained from experiments or CFD, supplemented by visualisation of distributed flow parameters.

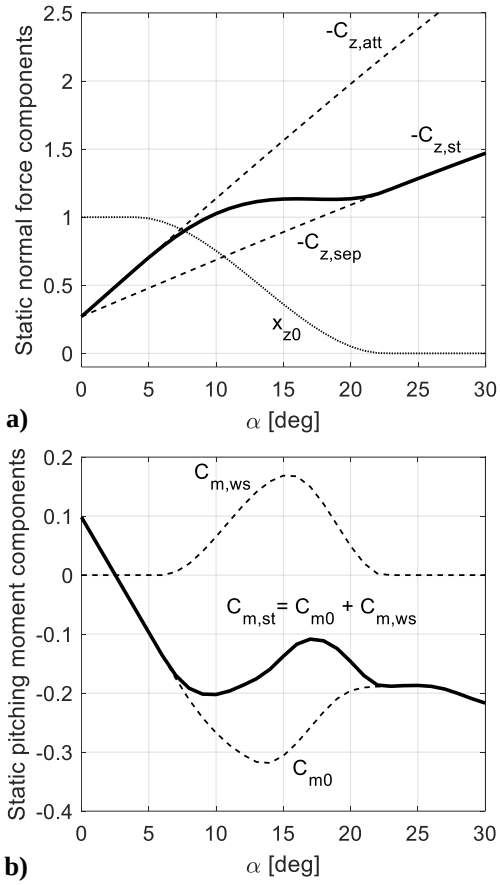

Fig. 2 Static unsteady aerodynamic components: normal force (a) and pitching moment (b).

C. GTT Implementation and Validation

The state-space approach outlined above is now applied to the NASA's Generic T-tail Transport (GTT) model. As the name suggests, the GTT represents a generic mid-size regional jet airliner with a T-tail configuration. Its aerodynamic data were collected from a series of low-speed sub-scale static and forced-oscillation wind tunnel and water tunnel flow visualisation tests, and some preliminary results have been reported in recent conferences [18-20]. The oscillatory tests were at one frequency and amplitude about each axis: reduced frequency for pitch-axis oscillations was 0.0158 and for the roll and yaw axes it was 0.094; the oscillation amplitudes were ±5° for the pitch axis and ±10° for the roll and yaw axes [19]. Computational fluid dynamics was also deployed to estimate the influence of the Reynolds number on the measured aerodynamics data, allowing the pitching moment and pitch damping data to be adjusted to represent the equivalent full-scale aircraft. For this study, we base our analysis on the original set of data from the sub-scale testing to construct a 4^{th}-order model that contains only longitudinal motions while neglecting the horizontal tailplane,

flaps and spoilers, which is deemed adequate for this study. All lateral-directional states and inputs are therefore zero. This 4th-order implementation contains 19 aerodynamics tables, which are 1D and 3D functions of angle-of-attack and of angle-of-attack/horizontal tailplane/elevator deflections.

In order to compare quasi-steady and unsteady aerodynamics modelling techniques, the following three models based on the GTT are created for this study:

- The 'quasi-steady' model is basically the original GTT but with the tabular data for static normal force and pitching moment replaced by spline functions as shown in Fig. 3 (as well as Fig. 2). The use of spline functions instead of look-up tables ensures consistency with the two unsteady models explained below while resulting in negligible difference comparing to the unmodified GTT.
- The 'nominal unsteady model' is augmented with two additional states x_z and x_m to describe the internal unsteady dynamics of C_z and C_m using the approach outlined in equations (7-10).
- A hypothetical highly-unsteady model is also examined to demonstrate the use of bifurcation analysis in studying unsteady aerodynamics phenomena. In this implementation, the time delay constants are both multiplied by a scale factor of 2.5 (i.e., τ_1 and τ_2 become $\Lambda\tau_1$ and $\Lambda\tau_2$, where Λ equals 2.5). This version is referred to as the 'Λ = 2.5' or 'highly-unsteady' model. Note that $\Lambda = 1$ is the nominal unsteady model.

It can be seen from Fig. 3 that the spline functions demonstrate a reasonable level of agreement between experimental and modelling results for static dependencies. The envelope boundaries for the normal force coefficients are quite well approximated as sinusoidal $C_{z,att}(\alpha) = a \sin\alpha$ and $C_{z,sep}(\alpha) = b \sin\alpha$, where a = –5.0, b = –2.4, and C_{z0} = –0.27. The upper limit $C_{z,sep}(\alpha)$ = –5 is close to the experimental data at small angles of attack below the stall, the lower limit $C_{z,sep}(\alpha)$ = –2.4 sin α is close to the experimental data beyond the stall to 90°, while the function $x_{z0}(\alpha)$ is responsible for the transition between the two envelope functions inside the stall region.

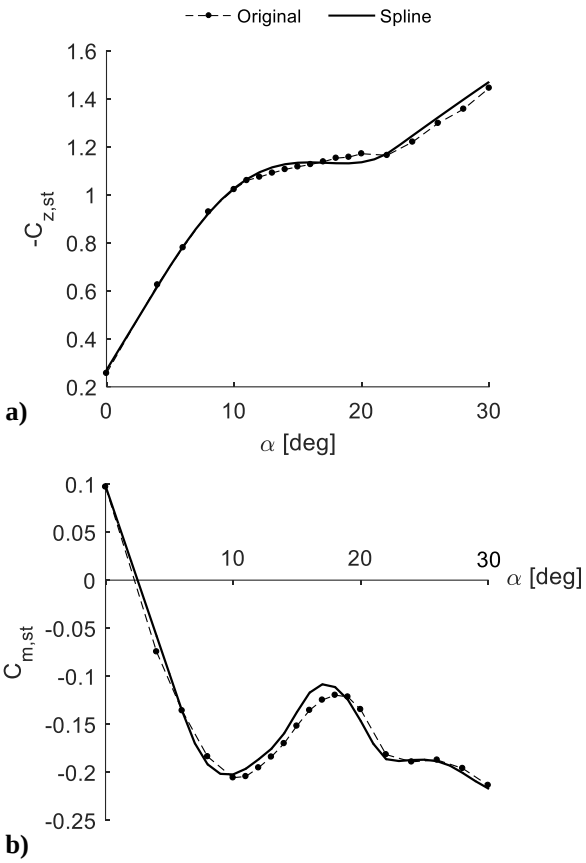

Fig. 3 Fitting of the static aerodynamic coefficients.

To verify the dynamic dependencies, the damping derivatives $C_{zq}^{*}(\alpha)$ and $C_{mq}^{*}(\alpha)$ of the quasi-steady and nominal unsteady models are now compared in Fig. 4. The simulation condition used to obtain these derivatives was selected to match the amplitude and frequency of angle-of-attack oscillations during wind tunnel experiments [19]: 5° in amplitude, f = 0.44 Hz in frequency at Re = 230,000 and flow speed V = 18 m/s. As the GTT chord length is c = 3.37 m, this gives a non-dimensionalised frequency of $2\pi fc/2V$ = 0.26. Correct identification of τ_1 and τ_2 should result in an unsteady model with damping derivatives $C_{zq}^{*}(\alpha)$ and $C_{mq}^{*}(\alpha)$ matching experimental data (quasi-steady modelling) in the condition specified above, especially in the stall region. The tuning process was done empirically, giving τ_1 = 4.5 and τ_2 = 3.5 for a reasonably good match. A more comprehensive approach would involve calculating τ_1 and τ_2 using a formal identification method to ensure the best fit between experimental and modelling result [23, 29], but this is beyond the scope of the paper.

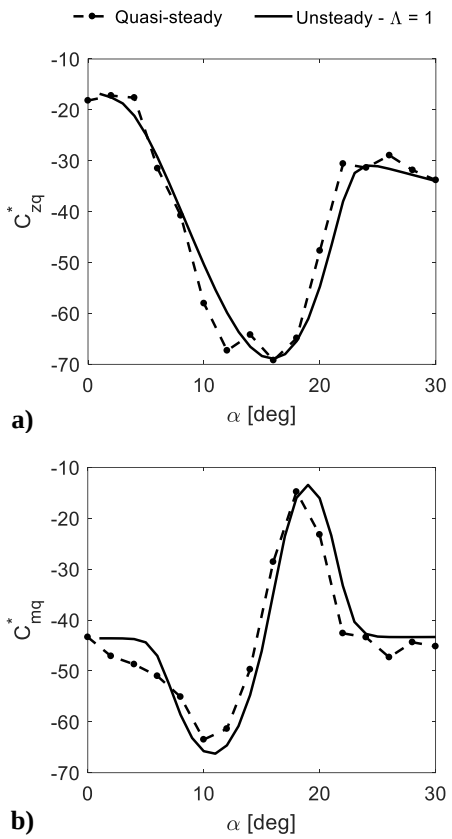

Fig. 4 Out-of-phase aerodynamic derivatives C^*_{zq} and C^*_{mq} from NASA wind tunnel tests [19] and simulated using the nominal unsteady aerodynamic model, obtained at frequency 0.44 Hz (reduced frequency: 0.26) and amplitude 5º.

It is worth noting that the values of τ_1 and τ_2 are similar to those obtained in [18] based on CFD simulations of the NASA Common Research Model (CRM) wing-body configuration (no empennage). The aerodynamic model structure for the normal force coefficient in [18] was identical to that obtained from equations (7-8) and the considered wing-body configuration excludes the interference with the horizontal tail. The dimensionless time constants found in [14] for this case were τ_1 = 4.86 and τ_2 = 3.89. These values are very close to those obtained in this study for the GTT aircraft, based on the NASA wind tunnel test data [19] and utilising the aerodynamic models (7-8) and (9-10), namely τ_1 = 4.5 and τ_2 = 3.5. This provides a reasonable independent verification of the obtained time constants in our study. It is interesting to note that for the full CRM geometry, with tailplane, the relaxation time for the model of the normal force coefficient shows an increase to τ_1 = 7.77, with no change in the delay τ_2 = 3.89 [18]. This increase in τ_1 is likely to account for the additional time for the downwash of the wing to act on the horizontal tail. The comparison

between the GTT and the CRM models provides qualitative evidence for the assumption that the wing-tail interaction can be neglected for the GTT.

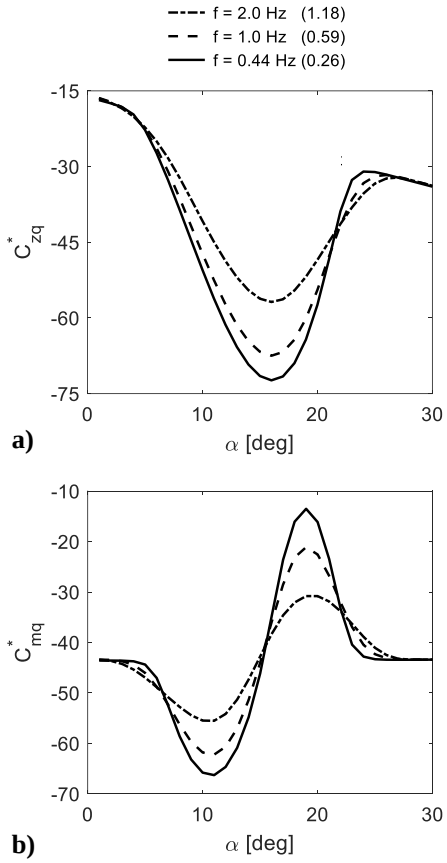

Fig. 5 Out-of-phase aerodynamic derivatives C_{zq}^{*} and C_{mq}^{*} of the unsteady models – obtained in simulated forced pitch oscillations with amplitude 5º and different frequencies.

Aerodynamic derivatives obtained from forced oscillation tests in a wind tunnel in a stall region usually depend on the frequency and amplitude of the oscillations. To illustrate such dependencies in the normal force and the pitching moment coefficients, Fig. 5 shows the estimated traditional rotary aerodynamic derivatives (3-4) for the GTT aircraft obtained as an out-of-phase aerodynamic derivative from simulated forced oscillation tests using the identified unsteady aerodynamic models (7-8) and (9-10). The peaks of the derivatives $C_{zq}^{*}(\alpha)$ and $C_{mq}^{*}(\alpha)$ in the stall region decrease in magnitude with increasing frequency ω, demonstrating a significant dependence on frequency. Such dependence on frequency makes the use of the quasi-steady aerodynamic model (3-4) problematic for simulations in the time domain in the stall region. The increase of frequency correlates with the increase of pitch rate amplitude q_{max} during forced oscillations executed at the same amplitude. This is why in [18, 20], for example, the damping

terms are the equivalent of equations (5-6), where frequency was replaced with angular rate q. Such modification of the quasi-steady aerodynamic model allows only the delay process in flow separation to be represented, while the relaxation process is not accounted for. The relaxation process is important in modelling of a vertical wind gust effect in the stall region [28].

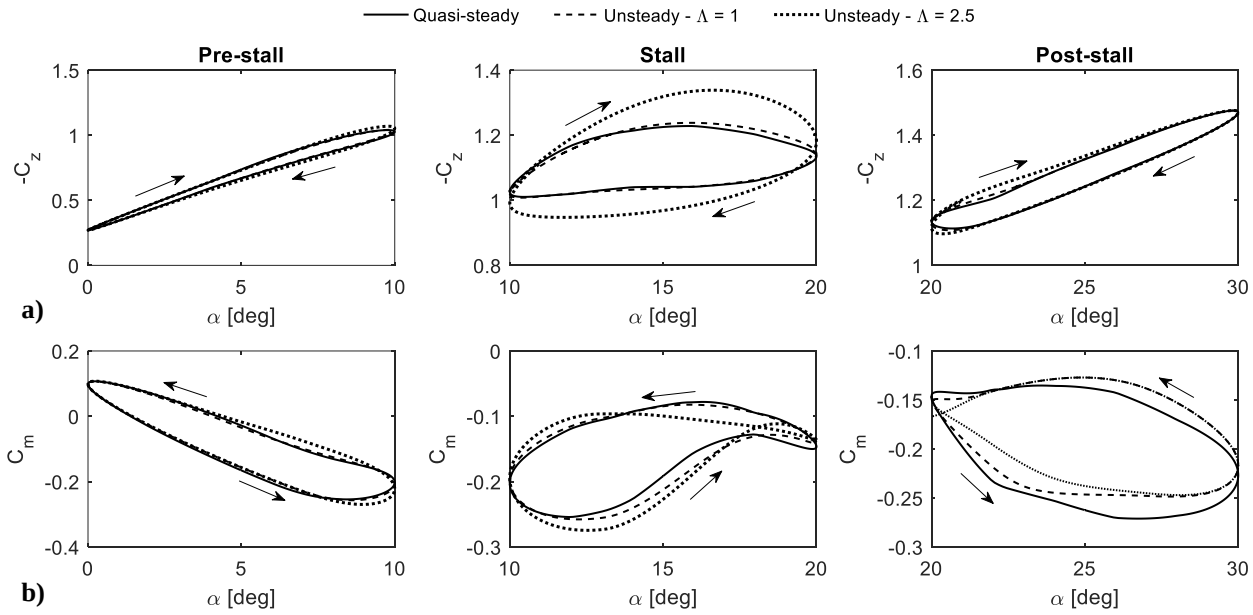

Fig. 6 Normal force (a) and pitching moment (b) variation in a sinusoidal α forcing at 0.44 Hz (reduced frequency: 0.26) and 5º amplitude – quasi-steady vs unsteady.

Now that the unsteady model has been verified to show a good match to the static and quasi-steady data under equivalent conditions, the effects of increasing the unsteady effects via the scaling factor Λ are examined. Fig. 6 compares the quasi-steady and unsteady force and moment coefficients when the angle-of-attack is subjected to a sinusoidal forcing. It can be observed that a good match is achieved between the quasi-steady and nominal-unsteady model. In fact, the unsteady effects only become more prominent by increasing Λ to 2.5, resulting in the differences seen around the stall region of the highly-unsteady model. Specifically, negative damping results in the twisted C_M loop of the Λ = 2.5 response as well as a thicker C_Z loop, which are indicative of more unsteady dynamics due to the increased delay in flow separation and reattachment. The choice of Λ = 2.5 in this study can be regarded as representative of a configuration in which the unsteady effects play a bigger role. For reference, the equivalent scaling factor in the case of the delta wing study in [23] is approximately Λ = 3.4.

It has been shown that the state-space method is a feasible alternative to the quasi-steady approach because their responses are more or less the same in regions where the quasi-steady data is known to be valid (i.e., for forced oscillation conditions equivalent to those used in the wind tunnel tests from which the quasi-steady dynamic derivatives were defined). Furthermore, a modification to the time delay constants using the scaling factor Λ brings out the unsteady aerodynamics effects of interest for an aircraft configuration in which there are stronger time dependencies; this facilitates a speculative study on the potential ramifications of unsteady effects on the aircraft's dynamics. These three models are now implemented on the fourth-order equations of motion to create the corresponding longitudinal flight dynamics models with four states $[\alpha, V, q, \theta]$ (plus two additional internal states x_z and x_m for the unsteady versions), which will be studied using bifurcation analysis in the sections to follow.

III. Bifurcation Analysis

The basics of bifurcation methods are illustrated in this section. For a comprehensive introduction to the topic, readers are referred to nonlinear dynamics textbooks such as [30, 31]. A simple example of unforced bifurcation analysis is provided in appendix A to demonstrate the method for readers new to the topic.

A. Unforced Bifurcation Analysis

Consider a general autonomous dynamical system of the form:

$$\dot{\boldsymbol{x}} = f(\boldsymbol{x}, \boldsymbol{u}) \tag{11}$$

where f is a vector of n smooth (differentiable) functions, $\boldsymbol{x}$ is the state vector of dimension $(n \times 1)$ and $\boldsymbol{u}$ is the input vector. In the context of open-loop flight dynamics, f is usually the equations of motion, $\boldsymbol{x}$ is the aircraft's states like α, V, and $\boldsymbol{u}$ contains the control inputs (i.e., elevator, aileron, etc.). The system is in equilibrium when:

$$\dot{\boldsymbol{x}} = \boldsymbol{0} \tag{12}$$

A periodic solution of period T exists when:

$$\boldsymbol{x}(t) = \boldsymbol{x}(t+T) \tag{13}$$

By solving equation (12) and/or equation (13), a map of steady states (either equilibrium or periodic) as functions of one of the control inputs in $\boldsymbol{u}$ can be generated. This map is referred to as a bifurcation diagram. We solve the equations numerically using continuation methods [32], which utilises a path-following algorithm to trace out a map of solutions as a parameter in $\boldsymbol{u}$ is varied. This varying parameter is referred to as the continuation parameter. Numerical continuation requires knowledge of at least one solution, which can be obtained by the user through the time-integration method (simulating the system in equation (11) long enough so that the states converge to their final values, assuming the system is stable) or Newton's method for equilibria. In many published works, the terms 'bifurcation analysis' and 'numerical continuation' are used interchangeably.

A bifurcation can be encountered in a nonlinear system, which reflects a qualitative change in the dynamics. Its mathematical definition is:

- For equilibrium solutions: when at least one eigenvalue of the system's Jacobian matrix $J = df/dx|_{x_0}$ (evaluated at the equilibrium point x_0) crosses the imaginary axis.

- For oscillatory solutions: when a Floquet multiplier crosses the unit circle.

Different types of bifurcations can lead to various nonlinear behaviours such as a limit cycle, multiple solutions for the same input, and hysteresis. A simple example of these concepts is provided in appendix A for readers who are new to the topic.

B. Harmonically-Forced Bifurcation Analysis/Nonlinear Frequency Response

Bifurcation analysis can be implemented on a harmonically-forced system, thereby generating a nonlinear Bode plot for frequency analysis. All ensuing motions are therefore periodic. The method to implement the harmonic forcing

term into bifurcation analysis is best explained by another simple example. Consider the following second-order nonlinear system:

$$\ddot{x} + c\dot{x} + kx + \epsilon x^3 = A\cos\omega t \tag{14}$$

This is the Duffing equation – a textbook example of nonlinear frequency response. In order to utilise the numerical continuation solver, equation (14) has to be re-written into autonomous first-order form (no t on the right-hand side). This results in the following fourth-order system:

$$\begin{aligned}
\dot{x}_1 &= x_2 \\
\dot{x}_2 &= -kx_1 - \epsilon {x_1}^3 - cx_2 + Ax_4 \\
\dot{x}_3 &= x_3 + \omega x_4 - x_3(x_3^2 + x_4^2) \\
\dot{x}_4 &= -\omega x_3 + x_4 - x_4(x_3^2 + x_4^2)
\end{aligned} \tag{15}$$

where $x_1 = x$, $x_2 = \dot{x}$, and $[x_3, x_4] = [\sin\omega t\,, \cos\omega t]$ (see appendix B for proof). A nonlinear frequency response is then obtained by setting ω as the continuation parameter, resulting in the Bode plot as shown in Fig. 7. Due to the nonlinear term, for $\epsilon > 0$, the resonance peak leans to the right and creates a region with multiple solutions and the possibility of hysteresis. This is demonstrated by forcing the system with a chirp signal (ω increasing or decreasing linearly). The data from time simulation is then superimposed on Fig. 7, which verifies the jump behaviour and hysteresis predicted by nonlinear frequency analysis.

All bifurcation analysis in this paper was performed using the Dynamical Systems Toolbox [33], which is the MATLAB/Simulink implementation of the numerical continuation software AUTO [34].

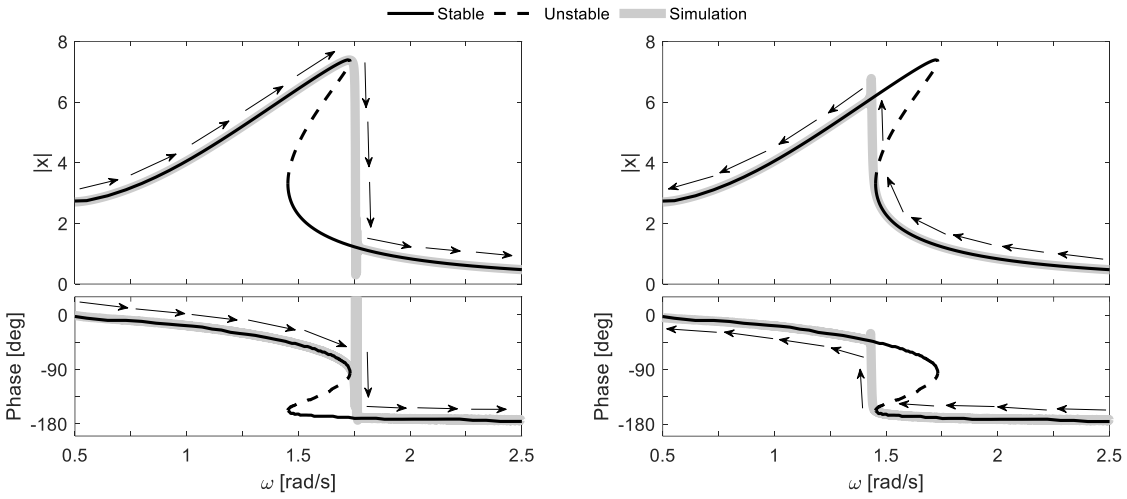

Fig. 7 Frequency response of the Duffing equation with time simulation data superimposed.

$[\boldsymbol{c}, \boldsymbol{k}, \boldsymbol{\epsilon}, \boldsymbol{A}]$ = [0.2, 1, 0.05, 2.5].

IV. Results and Discussions

We will now compare the flight dynamics characteristics of the NASA GTT using two different aerodynamic modelling methods: quasi-steady and unsteady. In both cases, the following standard fourth-order equations of motion for longitudinal dynamics are used:

$$\dot{\alpha} = \frac{1}{mV}\left[\frac{1}{2}\rho V^2 S(C_z \cos\alpha - C_x \sin\alpha) - T\sin\alpha + mg\cos(\theta - \alpha)\right] + q \tag{16}$$

$$\dot{V} = \frac{1}{m}\left[\frac{1}{2}\rho V^2 S(C_z \sin\alpha + C_x \cos\alpha) + T\cos\alpha - mg\sin(\theta - \alpha)\right] \tag{17}$$

$$\dot{q} = \frac{1}{2}\rho V^2 Sc\frac{C_m}{I_y} \tag{18}$$

$$\dot{\theta} = q \tag{19}$$

The aircraft parameters are shown in Table 1. The three total aerodynamic coefficients $[C_x, C_z, C_m]$ are made up of static and dynamic components.

Table 2 lists the data type for each static coefficient, and Table 3 summarises how the total component was calculated in the quasi-steady and unsteady models. Note that unsteady effects are not modelled for the axial force coefficient C_x in all cases.

Table 1. Aircraft parameters

S	wing area	70.08 m^2
c	mean aerodynamic chord	3.37 m
m	mass	25,332 kg
ρ	air density (at 10,000 ft)	0.90463 kg/m^3
I_y	pitch moment of inertia	1,510,624 kg m^2
T	thrust	22,000 N
g	gravitational acceleration	9.81 m/s^2

Table 2. Static aerodynamic data types

$C_{x,st}$	Tabular (not shown)
$C_{z,st}$	Splines (Fig. 3a)
$C_{m,st}$	Splines (Fig. 3b)

Table 3. Modelling methods of the three total aerodynamic coefficients

	Quasi-steady	Unsteady (Λ = 1 and 2.5)
C_x	Similar to eq. (3)	Similar to eq. (3)
C_z	eq. (3)	eq. (7-8)
C_m	eq. (4)	eq. (9-10)

A. Unforced Bifurcation Analysis

Fig. 8 shows the unforced bifurcation diagrams of the quasi-steady and unsteady GTT with the elevator deflection δ_e as the continuation parameter. The insets are magnified views of regions where limit cycles exist. Firstly, it is noted that Figs. 8a and b are very similar and suggest that dynamics of the quasi-steady and nominal-unsteady models are comparable. This observation is further verified in Fig. 9, which compares the pole positions of all equilibrium

solutions shown in the first two bifurcation diagrams (Figs. 8a and b). The rigid-body roots of the quasi-steady and nominal-unsteady models are comparable, although the latter model contains two additional real roots on the far-left due to the two internal states x_z and x_m. These two roots overlap each other and travel as a real pair (as opposed to a common complex-conjugate pair). Apart from this minor difference, the similar rigid-body roots verify that the state-space method is a valid alternative to quasi-steady modelling while also highlighting that unsteady aerodynamics in the current application (a T-tailed transport aircraft model that does not undergo rapid manoeuvres) is not sufficiently influential to require a time-dependent model. One can also make an opposite conclusion: that quasi-steady modelling is adequate for the GTT and possibly for any T-tail transport aircraft with negligible wing-tail coupling.

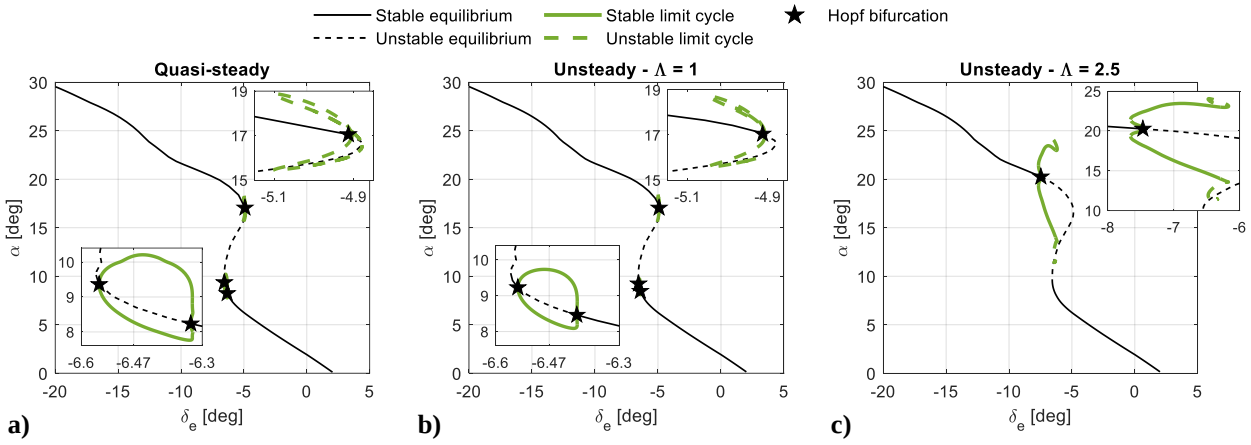

Fig. 8 Unforced bifurcation diagrams – elevator continuation.

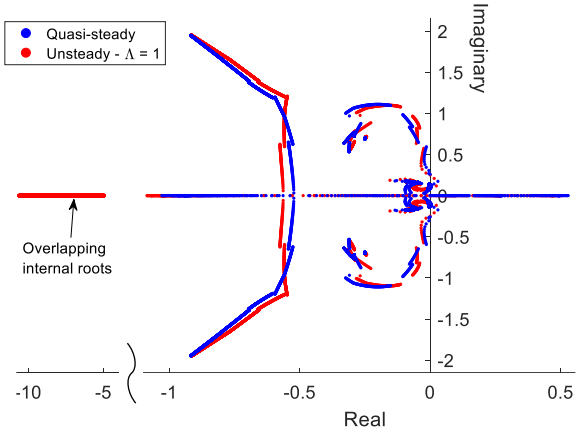

Fig. 9 Pole positions of all equilibrium solutions in Figs. 8a and b.

Figures 8a and b also feature a pair of Hopf bifurcations between 8.2° and 9.4° angle-of-attack. They give rise to a branch of stable limit cycles, meaning that the aircraft may encounter pitch oscillation in the region. This pair of Hopf bifurcations disappears in Fig. 8c when Λ is increased to 2.5. To verify the pitch oscillation, we trim the aircraft at δ_e = –6.3°, then step down to –6.47°. The resulting responses in Fig. 10 verify the limit cycle's existence in the quasi-steady and nominal-unsteady cases. For the Λ = 2.5 case, the aircraft is technically stable although marginally damped.

Another Hopf bifurcation is detected at a higher angle-of-attack. This occurs at around α = 17° for the first two cases, resulting in a branch of unstable limit cycles that collides with the unstable equilibrium branch (i.e., a global homoclinic bifurcation). These unstable limit cycles are not directly observable in time simulation. However, the similarity between figures 8a and b further emphasises that quasi-steady modelling is adequate to characterise the dynamics of the aircraft for the current application. When Λ is increased to 2.5, this Hopf bifurcation moves further to the left to reside at a higher angle-of-attack and create a branch of stable limit cycles that can be observed in time simulation – one of which is shown in Fig. 11 alongside a plot of how C_M varies with α throughout the oscillation. In the latter, it was found that the oscillation is linked to the damping loop in C_M being partly undamped, which in turn was a result of the highly unsteady aerodynamics. In other words, increasing Λ reduces damping at high angles-of-attack, which can lead to stability loss and pitch oscillation in extreme cases.

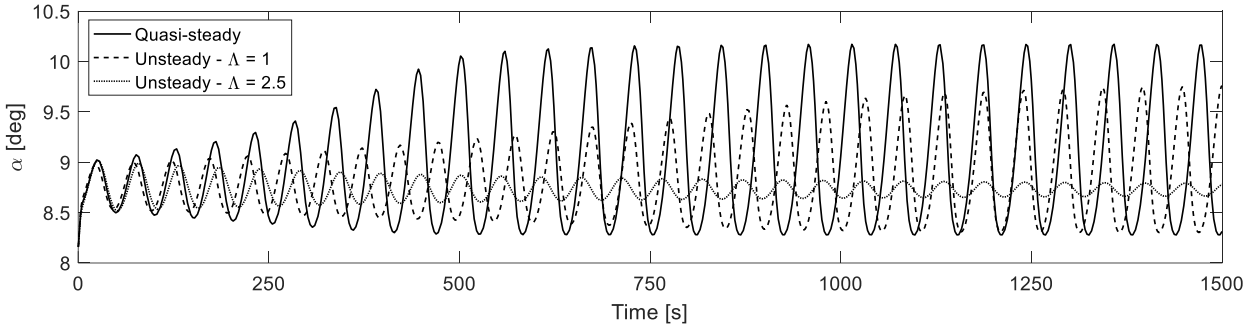

Fig. 10 Response to an elevator step from –6.3° to –6.47°.

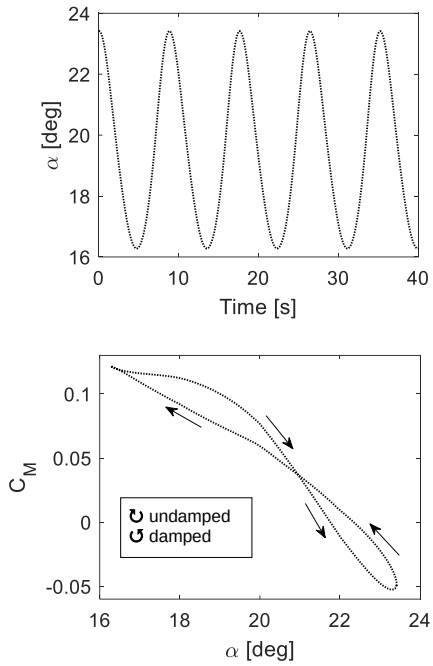

Fig. 11 A high-α stable limit cycle. [Λ, δ_e] = [2.5, –7°].

Finally, the reduced damping at high α is further highlighted by a large elevator step from –2° to –8° (Fig. 12). Based on the bifurcation diagrams, this manoeuvre equates to moving between the two stable trim points at 3.6° and 20.6° angle-of-attack. It can be seen from Fig. 12 that the quasi-steady and nominal-unsteady responses are very similar. On the other hand, the Λ = 2.5 case is very different in addition to being significantly less damped as inferred above.

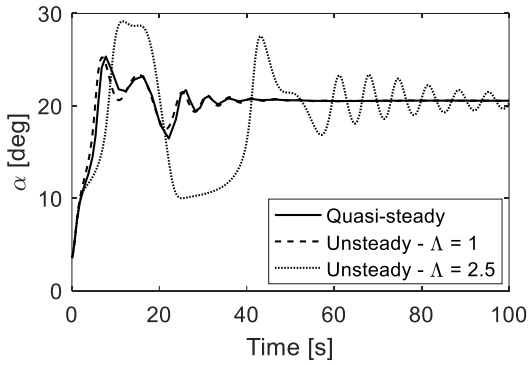

Fig. 12 Response to an elevator step from –2° to –8°.

In conclusion, unforced bifurcation analysis and time simulations verify that the state-space method provides a feasible alternative to the quasi-steady modelling approach. Conversely, it can also be said that, based on the cases studied

here, a quasi-steady model can be considered adequate for T-tail transport aircraft applications that do not undergo rapid manoeuvres. On the other hand, the responses become very different in the hypothetical highly-unsteady case, which underline the shortcomings of the quasi-steady method in instances where the unsteady effects are significant. The analyses also demonstrated the potential of combining the state-space modelling method with bifurcation analysis for studying the aircraft's flight dynamics in these highly nonlinear instances.

B. Forced Bifurcation Analysis

It has been shown that unforced bifurcation analysis provides valuable insights on the effects of unsteady aerodynamics on the aircraft dynamics especially at high angles-of-attack. However, this approach becomes less effective in closed-loop applications in which the controller provides stability. To illustrate this, consider a manoeuvre-demand system as shown Fig. 13a, where the input is demanded angle-of-attack α_d. Fig. 13b is the resulting unforced bifurcation diagram of the closed-loop system, which is identical for all three cases (quasi-steady, nominal-unsteady, and highly unsteady). This is because unforced bifurcation analysis only provides information on the equilibirum solutions. Since the controller already provides stability and allows us to trim the aircraft at any angle-of-attack within the elevator deflection range, the influence of unsteady aerodynamics is not noticable in Fig. 13b.

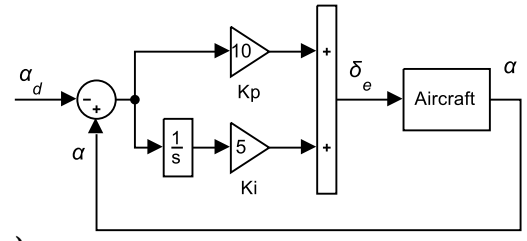

a)

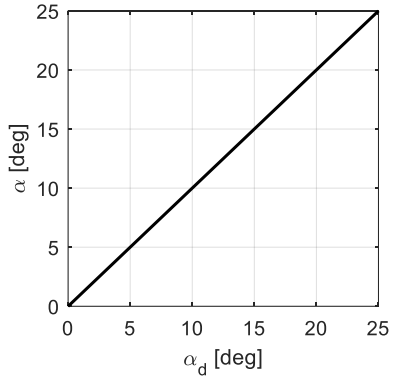

b)

Fig. 13 Closed-loop block diagram (a) and closed-loop unforced bifurcation diagram (b) (same for all cases).

In order to assess the controlled aircraft using bifurcation analysis, we will now employ the nonlinear frequency analysis method to observe the impact of the unsteady effects when the aircraft is non-stationary. The pilot input now takes the form $\alpha_d = 20 + 2\sin 2\pi f t$ (deg). This is equivalent to trimming the aircraft at 20° angle-of-attack, then apply a forcing input with amplitude 2° and frequency f (Hz). The resulting Bode plots are shown in Fig. 14. As before, the quasi-steady and nominal-unsteady cases are very similar, and both become unstable for a range of frequencies near resonance below 1 Hz. The resonance peak also includes a region of observable hysteresis; this feature is not discussed further as it is also observed in the quasi-steady model and is therefore caused by the nonlinearity in the tabular aerodynamic data (rather than the unsteady effects). When Λ is increased to 2.5, the unstable solution branch near resonance expands and covers a wider frequency range, up to 1.17 Hz. In all instances, stability is lost via a torus bifurcation, which gives rise to a large-amplitude quasi-periodic oscillation. We verify this by comparing the forced responses at 1 Hz in time simulation (Fig. 15). As predicted by nonlinear frequency analysis, this stick pumping results in very small-amplitude oscillations at exactly 1 Hz for the quasi-steady and nominal-unsteady responses. However, the Λ = 2.5 simulation is remarkably different. In addition to having an extremely large amplitude, the oscillation is quasi-periodic at around 0.14 Hz, which is significantly lower than the 1 Hz input. This behaviour marks a degraded controller performance. Since the quasi-periodic (unstable) region expands as Λ increases, it can be said that unsteady aerodynamics can negatively affect the controller's performance in a manner that cannot be detected using the quasi-steady modelling approach and even unforced bifurcation analysis with full unsteady aerodynamics modelling. These shortcomings can be addressed by using forced bifurcation analysis.

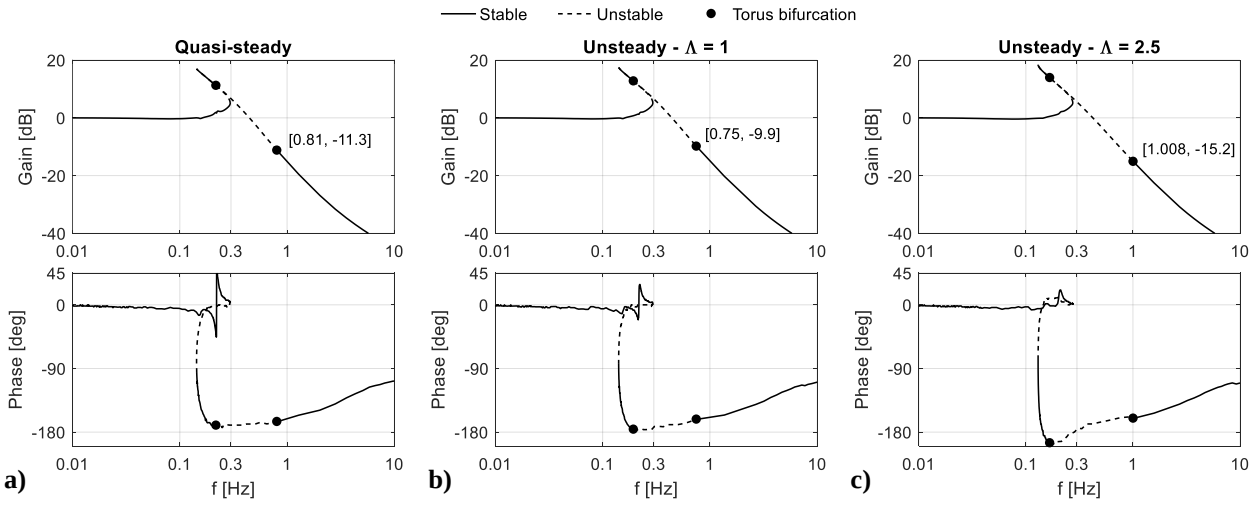

Fig. 14 α-to-α_d frequency responses. $\alpha_d = 20 + 2\,sin\,2\pi f t$ (deg). For clarity, not all bifurcations are shown.

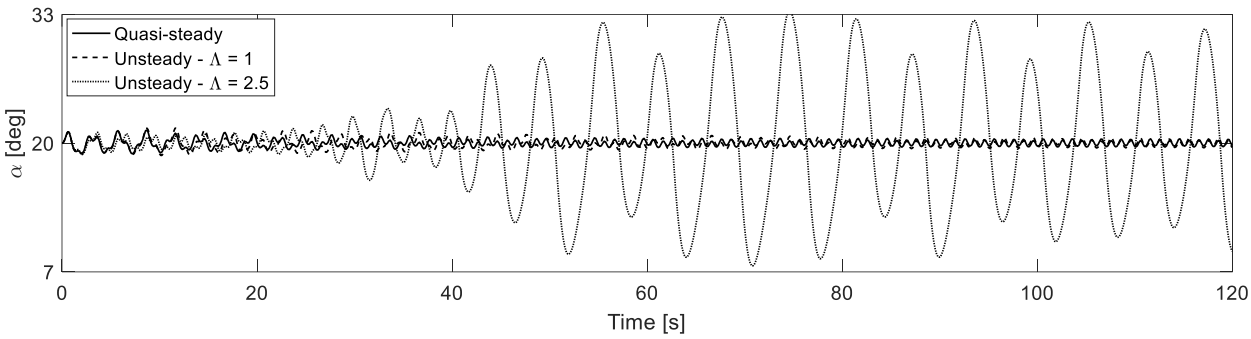

Fig. 15 Forced responses at 1 Hz.

The dynamics at resonance is also affected by the presence of unsteady aerodynamics. To illustrate, consider the motions during a large oscillation at 0.30 Hz forcing, for which there are no stable (period-1) solutions in all three cases according to the nonlinear Bode plots. The resulting phase plots in Fig. 16 show chaotic oscillations for the first two cases and period-2 stable for the highly unsteady one. As before, the dynamics of the quasi-steady and $\Lambda = 1$ models are qualitatively similar, despite the large-amplitude oscillations. This further validates the adequacy of the state-space modelling method for the GTT.

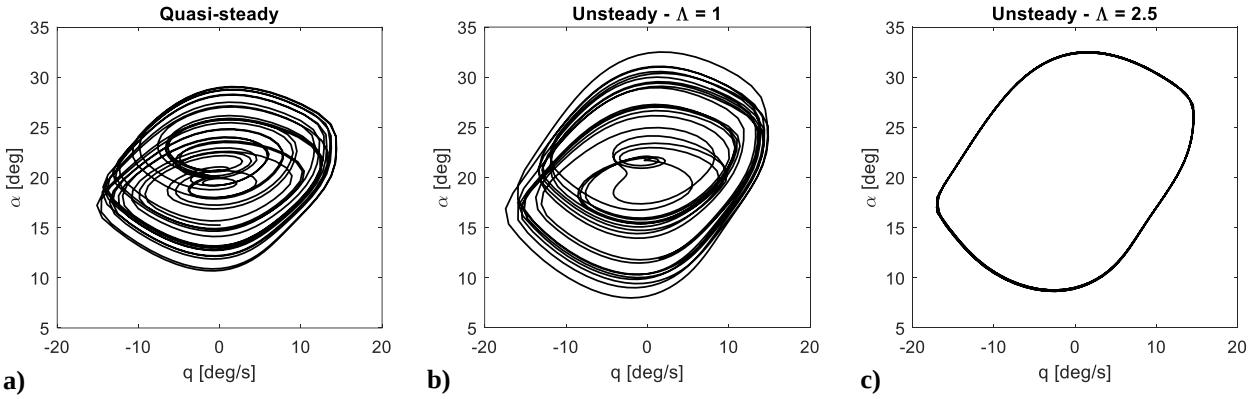

Fig. 16 Phase plots at 0.30 Hz forcing, showing trajectories between 500s and 600s.

V. Conclusion

This paper presents one of the first attempts at combining the state-space aerodynamic modelling method with bifurcation analysis for a fixed-wing aircraft, and at extending this to investigate the effects of the aerodynamic

modelling on transient behaviour via nonlinear frequency responses generated using numerical continuation. Whilst previous studies were limited to assessments of only aerodynamic characteristics, it has been shown here that the influence of unsteady aerodynamics relative to a quasi-steady formulation in the context of longitudinal dynamics and control can be directly evaluated using bifurcation analysis.

The study starts with the longitudinal quasi-steady aerodynamic model provided by NASA Langley for the sub-scale GTT configuration, based on wind tunnel data. A state-space unsteady model is then derived to match the quasi-steady static and oscillatory lift and pitching moment characteristics and to also capture time-dependent separated flow effects. The two models were compared, in respect of aerodynamic responses and also flight dynamic responses via bifurcation analysis and time histories. In addition, harmonically forced bifurcation analysis was implemented to generate nonlinear frequency response plots. This approach provides another way to assess unsteady aerodynamic effects in terms of stability and control.

Combining the state-space aerodynamic modelling method and bifurcation analysis allows the following observations to be made, which have not been thoroughly assessed previously:

- Quasi-steady aerodynamic modelling is adequate for the longitudinal NASA GTT model, and potentially more generally for other T-tail transport aircraft that do not undergo rapid manoeuvring.
- Likewise, the state-space modelling approach is a feasible alternative that provides comparable responses in regions where the quasi-steady results are known to be valid, and yields frequency dependence that is missing from the quasi-steady form.

The above was also applied to the longitudinal behaviour of a hypothetical highly-unsteady aircraft model with time delay parameters chosen to resemble a delta wing configuration found in high-performance fighter aircraft. In this case, the aircraft's open- and closed-loop performance was shown to be severely degraded, especially at high angles-of-attack and while transitioning between the stall and post-stall regimes. In this study, unforced bifurcation analysis detected the formation of stable limit cycles in the post-stall regime, and harmonically forced bifurcation analysis confirmed the significant reduction in pitch damping via the widened resonance region. Both of these indicate severely

degraded flying qualities caused by the aerodynamic phenomena that cannot be reflected using the traditional quasi-steady modelling technique. Furthermore, this suggests that a representative mathematical model of these highly manoeuvrable platforms must account for unsteady aerodynamic effects in order to properly capture the stall and post-stall behaviours. To this end, the combination of state-space aerodynamic modelling and bifurcation analysis presents a powerful alternative to traditional quasi-steady modelling and conventional analysis methods.

Appendices

A. An Example of Unforced Bifurcation Analysis

Consider the following simple dynamical system:

$$\ddot{x} + (x^2 - m)\dot{x} + x = 0 \tag{A1}$$

This a variation of the Van der Pol oscillator. Nonlinearity comes from the damping term $(x^2 - m)$. It can be seen that an equilibrium solution exists at the origin, and that increasing m beyond 0 destabilises this equilibrium point due to the negative damping. Indeed, Fig. A17 shows the time simulation and phase plot at m = 1 with non-zero initial conditions. The system enters a stable self-sustained oscillation that is only suppressed by the increased damping as x moves away from the origin. Consequently, its phase plot shows a closed-trajectory (i.e., a limit cycle).

Fig. A18a is the bifurcation diagram of equation (A1) with m as the continuation parameter. Stable equilibrium solutions exist for all negative m. When m exceeds 0, a Hopf bifurcation is detected, which led to a family of stable limit cycle that increases in amplitude with increasing m (i.e., damping becomes increasingly negative). The link between the limit cycle amplitude and m can be verified by running a time simulation with m reducing linearly from a high value at a rate of $0.26t$. Data from this time simulation (plotted in terms of m rather than t) are superimposed on Fig. A18a, and match the prediction made by bifurcation analysis. The 3D projection of the phase plot is shown in Fig. A18b.

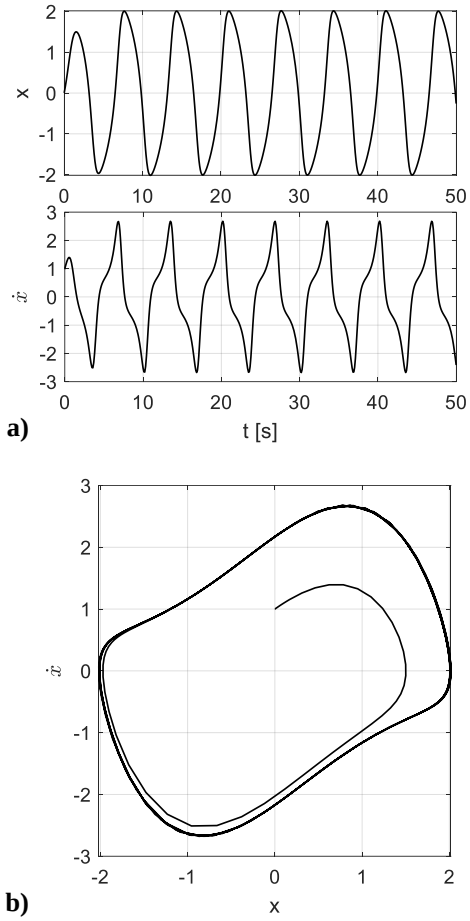

Fig. A17 Time simulation (a) and phase plot (b) of equation (A1).

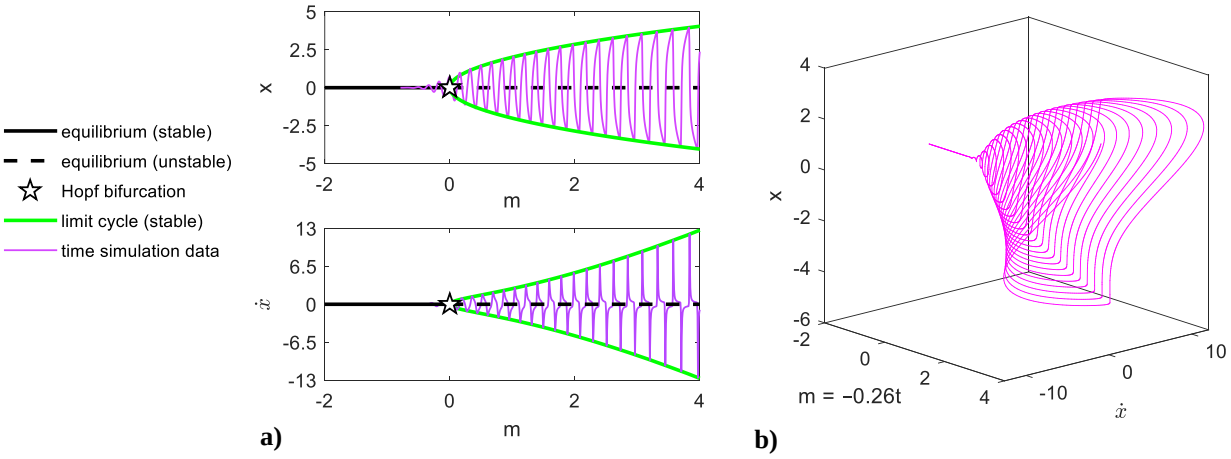

Fig. A18 Bifurcation diagram of the modified Van der Pol oscillator with simulated response superimposed (a). 3D projection of the simulation data (b)

B. Proof of the Harmonic Oscillator Equations

The third and fourth states derivatives in equations (15) are reproduced below:

$$\begin{aligned} \dot{x}_3 &= \ x_3 + \omega x_4 - x_3(x_3^2 + x_4^2) \\ \dot{x}_4 &= -\omega x_3 + x_4 - x_4(x_3^2 + x_4^2) \end{aligned} \tag{A2}$$

Introducing the complex variable $z = x_4 + ix_3$. We have:

$$|z|^2 = x_3^2 + x_4^2 \tag{A3}$$

and

$$\begin{aligned} \dot{z} &= \dot{x}_4 + i\dot{x}_3 \\ \dot{z} &= [-\omega x_3 + x_4 - x_4(x_3^2 + x_4^2)] + i[x_3 + \omega x_4 - x_3(x_3^2 + x_4^2)] \\ \dot{z} &= (x_4 + ix_3) - (x_3^2 + x_4^2)(x_4 + ix_3) + i\omega(x_4 + ix_3) \\ \dot{z} &= z - |z|^2 z + i\omega z \\ \dot{z} &= z(1 - |z|^2 + i\omega) \end{aligned} \tag{A4}$$

Now transform z to its polar form of $z = re^{i\theta}$, giving $|z|^2 = r^2$. Substitute these in equation (A4):

$$\dot{z} = \ re^{i\theta}(1 - r^2 + i\omega) \tag{A5}$$

Furthermore, the first derivative of $z = re^{i\theta}$ is:

$$\dot{z} = \ \dot{r}e^{i\theta} + i\dot{\theta}re^{i\theta} = e^{i\theta}(\dot{r} + i\dot{\theta}r) \tag{A6}$$

Equating (A5) and (A6) and cancelling $e^{i\theta}$ gives:

$$r(1-r^2)+i\omega r = \dot{r}+i\dot{\theta}r \tag{A7}$$

Therefore:

$$\begin{cases}\dot{r}=r(1-r^2)\\ \dot{\theta}=\omega\end{cases} \tag{A8}$$

It can be seen that $r=1$ gives $\dot{r}=0$. In this instance, the system becomes:

$$\begin{cases}\dot{r}=0\\ \dot{\theta}=\omega\end{cases} \tag{A9}$$

which describes a phasor of constant radius 1 and constant angular velocity ω rad/s. Its real and imaginary components are $x_4=\cos\omega t$ and $x_3=\sin\omega t$, respectively. To ensure that $r=1$ at the start of the simulation, set $x_3(t=0)=0$ and $x_4(t=0)=1$.

We can now couple the states x_3 and/or x_4 into the system's equations of motion to generate the harmonic forcing term in autonomous form for bifurcation analysis.

Acknowledgments

The first author is partially funded by the University of Bristol's Alumni Grant. The second author is funded by the EU H2020 SAFEMODE project (grant agreement ID: 814961). We are grateful to NASA Langley Research Center, specifically Kevin Cunningham and Gautam Shah, for providing the GTT model aerodynamic data.

References

1. Bryan, G. H., *Stability in Aviation: An Introduction to Dynamical Stability as Applied to the Motions of Aeroplanes*, chapter II, Macmillan and Company, Limited, London, 1911.

2. Heller, M., Holmberg, J., and David, R. "Significance of Unsteady Aerodynamic Effects in F/A-18C/D Pitching Moment", *AIAA Atmospheric Flight Mechanics Conference and Exhibit*, AIAA Paper AIAA-2006-6485, 2006. doi: 10.2514/6.2006-6485

3. Abzug, M. J., and Larrabee, E. E., *Airplane Stability and Control: A History of the Technologies that Made Aviation Possible*, 2, Cambridge Aerospace Series, Cambridge University Press, Cambridge, 2002. doi: DOI: 10.1017/CBO9780511607141

4. Abramov, N. B., Goman, M. G., Khrabrov, A. N., and Soemarwoto, B. I. "Aerodynamic Modeling for Poststall Flight Simulation of a Transport Airplane", *Journal of Aircraft,* Vol. 56, No. 4, 2019, pp. 1427-1440. doi: 10.2514/1.C034790

5. Murphy, P. C., and Klein, V. "Estimation of Unsteady Aerodynamic Models from Dynamic Wind Tunnel Data", *Assessment of Stability and Control Prediction Methods for NATO Air and Sea Vehicles*, NATO RTO Paper RTO-MP-AVT-189, 2011. doi: 10.14339/RTO-MP-AVT-189

6. Greenwell, D. "A Review of Unsteady Aerodynamic Modelling for Flight Dynamics of Manoeuvrable Aircraft", *AIAA Atmospheric Flight Mechanics Conference and Exhibit*, Vol. AIAA 2004-5276, pp. 2004. doi: 10.2514/6.2004-5276

7. Kyle, H., Lowenberg, M., and Greenwell, D. "Comparative Evaluation of Unsteady Aerodynamic Modelling Approaches", *AIAA Atmospheric Flight Mechanics Conference and Exhibit*, Vol. AIAA 2004-5272, pp. 2004. doi: 10.2514/6.2004-5272

8. Mehra, R., and Carroll, J. "Bifurcation analysis of aircraft high angle-of-attack flight dynamics", *6th Atmospheric Flight Mechanics Conference*, AIAA Paper 80-1599, 1980. doi: 10.2514/6.1980-1599

9. Carroll, J. V., and Mehra, R. K. "Bifurcation Analysis of Nonlinear Aircraft Dynamics", *Journal of Guidance, Control, and Dynamics,* Vol. 5, No. 5, 1982, pp. 529-536. doi: 10.2514/3.56198

10. Jahnke, C. C., and Culick, F. E. C. "Application of bifurcation theory to the high-angle-of-attack dynamics of the F-14", *Journal of Aircraft,* Vol. 31, No. 1, 1994, pp. 26-34. doi: 10.2514/3.46451

11. Guicheteau, P. "Bifurcation theory: a tool for nonlinear flight dynamics", *Philosophical Transactions of the Royal Society of London. Series A: Mathematical, Physical and Engineering Sciences,* Vol. 356, No. 1745, 1998, pp. 2181-2201. doi: 10.1098/rsta.1998.0269

12. Kwatny, H. G., Dongmo, J.-E. T., Chang, B.-C., Bajpai, G., Yasar, M., and Belcastro, C. "Nonlinear Analysis of Aircraft Loss of Control", *Journal of Guidance, Control, and Dynamics,* Vol. 36, No. 1, 2013, pp. 149-162. doi: 10.2514/1.56948

13. Gill, S. J., Lowenberg, M. H., Neild, S. A., Krauskopf, B., Puyou, G., and Coetzee, E. "Upset Dynamics of an Airliner Model: A Nonlinear Bifurcation Analysis", *Journal of Aircraft,* Vol. 50, No. 6, 2013, pp. 1832-1842. doi: 10.2514/1.C032221

14. Rezgui, D., Lowenberg, M. H., Jones, M., and Monteggia, C. "Continuation and Bifurcation Analysis in Helicopter Aeroelastic Stability Problems", *Journal of Guidance, Control, and Dynamics,* Vol. 37, No. 3, 2014, pp. 889-897. doi: 10.2514/1.60193

15. Nguyen, D. H., Lowenberg, M. H., and Neild, S. A. "Frequency-Domain Bifurcation Analysis of a Nonlinear Flight Dynamics Model", *Journal of Guidance, Control, and Dynamics*, Vol. 44, No. 1, 2021, pp. 138-150. doi: 10.2514/1.G005197

16. Nguyen, D. H., Lowenberg, M. H., and Neild, S. A. "Effect of Actuator Saturation on Pilot-Induced Oscillation: a Nonlinear Bifurcation Analysis", *Journal of Guidance, Control, and Dynamics*, Vol. 44, No. 5, 2021, pp. 1018-1026. doi: 10.2514/1.G005840

17. "Loss of Control on Approach, Colgan Air, Inc., Operating as Continental Connection Flight 3407, Bombardier DHC-8-400, N200WQ, Clarence Center, New York, February 12, 2009." National Transportation Safety Board, Washington, DC, 2010.

18. Cunningham, K., Shah, G. H., Hill, M. A., Pickering, B. P., Litt, J. S., and Norin, S. "A Generic T-tail Transport Airplane Simulation for High-Angle-of-Attack Dynamics Modeling Investigations", *2018 AIAA Modeling and Simulation Technologies Conference*, AIAA Paper AIAA-2018-1168, 2018. doi: 10.2514/6.2018-1168

19. Cunningham, K., Shah, G. H., Frink, N. T., McMillin, S. N., Murphy, P. C., Brown, F. R., Hayes, P. J., Shweyk, K. M., and Nayani, S. N. "Preliminary Test Results for Stability and Control Characteristics of a Generic T-tail Transport Airplane at High Angle of Attack", *2018 AIAA Atmospheric Flight Mechanics Conference*, AIAA Paper AIAA-2018-0529, 2018. doi: 10.2514/6.2018-0529

20. Cunningham, K., Shah, G. H., Murphy, P. C., Hill, M. A., and Pickering, B. "Pilot Sensitivity to Simulator Flight Dynamics Model Formulation for Stall Training", *AIAA Scitech 2019 Forum*, AIAA Paper AIAA-2019-0717, 2019. doi: 10.2514/6.2019-0717

21. McMillin, S. N., Frink, N. T., Murphy, P. C., Cunningham, K., Shah, G. H., and Nayani, S. N. "Computational Study of a Generic T-tail Transport", *AIAA Scitech 2019 Forum*, AIAA Paper AIAA 2019-0036, 2019. doi: 10.2514/6.2019-0036

22. Goman, M. G., and Khrabrov, A. N. "State-space representation of aerodynamic characteristics of an aircraft at high angles of attack", *Journal of Aircraft*, Vol. 31, No. 5, 1994, pp. 1109-1115. doi: 10.2514/3.46618

23. Abramov, N., Goman, M., and Khrabrov, A. "Aircraft Dynamics at High Incidence Flight with Account of Unsteady Aerodynamic Effects", *AIAA Atmospheric Flight Mechanics Conference and Exhibit*, Paper AIAA 2004-5274, 2004. doi: 10.2514/6.2004-5274

24. Khrabrov, A., Vinogradov, Y., and Abramov, N. "Mathematical Modelling of Aircraft Unsteady Aerodynamics at High Incidence with Account of Wing-Tail Interaction", *AIAA Atmospheric Flight Mechanics Conference and Exhibit*, AIAA Paper AIAA 2004-5278, 2004. doi: 10.2514/6.2004-5278

25. Pattinson, J., Lowenberg, M. H., and Goman, M. G. "Investigation of Poststall Pitch Oscillations of an Aircraft Wind-Tunnel Model", *Journal of Aircraft*, Vol. 50, No. 6, 2013, pp. 1843-1855. doi: 10.2514/1.C032184

26. Luchtenburg, D. M., Rowley, C. W., Lohry, M. W., Martinelli, L., and Stengel, R. F. "Unsteady High-Angle-of-Attack Aerodynamic Models of a Generic Jet Transport", *Journal of Aircraft*, Vol. 52, No. 3, 2015, pp. 890-895. doi: 10.2514/1.C032976

27. Williams, D. R., Reißner, F., Greenblatt, D., Müller-Vahl, H., and Strangfeld, C. "Modeling Lift Hysteresis on Pitching Airfoils with a Modified Goman–Khrabrov Model", *AIAA Journal,* Vol. 55, No. 2, 2017, pp. 403-409. doi: 10.2514/1.J054937

28. Sedky, G., Jones, A. R., and Lagor, F. D. "Lift Regulation During Transverse Gust Encounters Using a Modified Goman–Khrabrov Model", *AIAA Journal,* Vol. 58, No. 9, 2020, pp. 3788-3798. doi: 10.2514/1.J059127

29. Greenwell, D., Khrabrov, A., Goman, M., and Abramov, N. "Two-step linear regression method for identification of high incidence unsteady aerodynamic model", *AIAA Atmospheric Flight Mechanics Conference and Exhibit*, Paper AIAA 2001-4080, 2001. doi: 10.2514/6.2001-4080

30. Strogatz, S. H., *Nonlinear Dynamics and Chaos: with Applications to Physics, Biology, Chemistry, and Engineering*, Addison–Wesley, Reading, MA, 1994.

31. Kuznetsov, I. A., *Elements of applied bifurcation theory*, 3rd ed., Applied mathematical sciences ; v. 112, Springer, New York, 2004.

32. Krauskopf, B., Osinga, H. M., and Galán-Vioque, J., *Numerical continuation methods for dynamical systems: path following and boundary value problems*, Understanding Complex Systems, chapter 1, Springer, Dordrecht, 2007. doi: 10.1007/978-1-4020-6356-5

33. Coetzee, E., Krauskopf, B., and Lowenberg, M. H. "The Dynamical Systems Toolbox: Integrating AUTO into Matlab", *16th US National Congress of Theoretical and Applied Mechanics*, USNCTAM Paper USNCTAM2010-827, 2010.

34. Doedel, E. J. "*AUTO-07P, Continuation and Bifurcation Software for Ordinary Differential Equations, Ver. 07P*", http://www.macs.hw.ac.uk/~gabriel/auto07/auto.html [retrieved 8 April 2021].